Open Research Online

The Open University's repository of research publications and other research outputs

Comparative performance of airyscan and structured illumination superresolution microscopy in the study of the surface texture and 3D shape of pollen

Journal Item

How to cite:

Sivaguru, Mayandi; Urban, Michael A.; Fried, Glenn; Wesseln, Cassandra J.; Mander, Luke and Punyasena, Surangi W. (2018). Comparative performance of airyscan and structured illumination superresolution microscopy in the study of the surface texture and 3D shape of pollen. Microscopy Research and Technique, 81(2) pp. 101–114.

For guidance on citations see FAQs.

© 2016 Wiley Periodicals, Inc.

https://creativecommons.org/licenses/by-nc-nd/4.0/

Version: Version of Record

Link(s) to article on publisher's website:
http://dx.doi.org/doi:10.1002/jemt.22732

Copyright and Moral Rights for the articles on this site are retained by the individual authors and/or other copyright owners. For more information on Open Research Online's data policy on reuse of materials please consult the policies page.

oro.open.ac.uk

Received: 19 January 2016 | Revised: 3 May 2016 | Accepted: 5 July 2016
DOI 10.1002/jemt.22732

RESEARCH ARTICLE

WILEY

Comparative performance of airyscan and structured illumination superresolution microscopy in the study of the surface texture and 3D shape of pollen

Mayandi Sivaguru[1] | Michael A. Urban[2] | Glenn Fried[1] | Cassandra J. Wesseln[3] | Luke Mander[4] | Surangi W. Punyasena[2,3]

[1]Institute for Genomic Biology, University of Illinois, 1206 West Gregory Drive, Urbana, Illinois, 61801

[2]Department of Plant Biology, University of Illinois, 505 South Goodwin Avenue, Urbana, Illinois, 61801

[3]Program in Ecology, Evolution, and Conservation Biology, University of Illinois, 505 South Goodwin Avenue, Urbana, Illinois, 61801

[4]Department of Environment Earth and Ecosystems, The Open University, Milton Keynes, MK7 6AA, United Kingdom

Correspondence
Surangi W. Punyasena, Department of Plant Biology, University of Illinois, 505 South Goodwin Avenue, Urbana, Illinois, 61801.
Email: punyasena@life.illinois.edu

Review Editor: Prof. Alberto Diaspro

Abstract

The visualization of taxonomically diagnostic features of individual pollen grains can be a challenge for many ecologically and phylogenetically important pollen types. The resolution of traditional optical microscopy is limited by the diffraction of light (250 nm), while high resolution tools such as electron microscopy are limited by laborious preparation and imaging workflows. Airyscan confocal superresolution and structured illumination superresolution (SR-SIM) microscopy are powerful new tools for the study of nanoscale pollen morphology and three-dimensional structure that can overcome these basic limitations. This study demonstrates their utility in capturing morphological details below the diffraction limit of light. Using three distinct pollen morphotypes (*Croton hirtus*, *Dactylis glomerata*, and *Helianthus* sp.) and contrast-enhancing fluorescent staining, we were able to assess the effectiveness of the Airyscan and SR-SIM. We further demonstrate that these new superresolution methods can be easily applied to the study of fossil pollen material.

KEYWORDS
confocal, fluorescence, fossil pollen morphology, SR-SIM

1 | INTRODUCTION

Palynologists classify pollen grains into taxonomic groups on the basis of morphological features. These include the shape of the pollen grain, the number and arrangement of any apertures, and the ornamentation of the pollen surface (Punt, Hoen, Blackmore, Nilsson, & Le Thomas, 2007; Traverse, 2007). The choice of microscopy technique affects the morphological detail that can be observed and the accuracy of the resulting taxonomic classification (Mander & Punyasena, 2014). Palynologists select a microscopy method according to the nature of the study and the types of morphological features they aim to investigate (Sivaguru, Mander, Fried, & Punyasena, 2012; Mander & Punyasena, 2014). Research that relies on the rapid identification of hundreds to thousands of individual pollen grains (such as the reconstruction of vegetation history through the geologic past or the generation of pollen counts for allergy forecasts) primarily involves the use of brightfield transmitted light microscopy (Fægri, Iversen, & Kaland, 1992; Traverse, 2007). This technique has been the backbone of palynology from its inception, and the terminology that is used to describe the morphology of pollen grains is based principally on morphological features that can be inspected using brightfield transmitted light microscopy (Punt et al., 2007).

However, the resolution of conventional optical microscopy methods, which includes brightfield transmitted light microscopy, is limited by the diffraction of light in most practical situations (Heintzmann & Ficz, 2006; Weiss, 2000). This "diffraction limit" means that optical techniques are unable to capture morphological features that are less than 200–250 nm in size. In certain plant groups, such as the grasses, the morphological features that distinguish the pollen of different species are far smaller than 200 nm (Andersen & Bertelsen, 1972; Chaturvedi, Datta, & Nair, 1998; Mander, Li, Mio, Fowlkes, & Punyasena, 2013; Page, 1978; Peltre, Cerceau-Larrival, Hideux, Abadie, & David,

 © 2016 Wiley Periodicals, Inc.

1987). In these cases, the diffraction limit represents a fundamental barrier to the process of classification (Mander & Punyasena, 2014).

Detailed investigations of pollen morphology, therefore, are supplemented by electron microscopy (EM) techniques such as scanning electron microscopy (SEM) and transmitted electron microscopy (TEM) (Fægri et al., 1992; Traverse, 2007; Hesse et al., 2009). In contrast to most optical microscopy methods, SEM and TEM provide the highest-resolution visualizations of pollen morphology. SEM captures the surface details of a pollen grain, with a spatial resolution of less than 5 nm (Mander et al., 2013). Detailed analysis of the interior of the pollen wall is possible using complementary TEM images of microtome sections. TEM can reach resolutions of up to 0.5 nm (Reimer & Kohl, 2008), although that extreme degree of resolution is not required for standard pollen analyses. The high magnification of EM makes it indispensable to many morphological studies of pollen material. The "gold-standard" approach to pollen classification requires linking the generalized morphology observed under transmitted brightfield light with the finer features evident in SEM and TEM images. Detailed observations under EM are required to test hypotheses of biologic affinity and to confirm observations made using transmitted light. However, the isolation and imaging of pollen grains with EM can be laborious and is therefore only undertaken with a handful of specimens within a pollen sample. Routine imaging of a large number of pollen grains using EM is, therefore, not standard practice.

Optical methods with superresolution capabilities—which allow observation of morphological features below the diffraction limit, and thereby reduce or replace the need for electron microscopy—would therefore be transformational to the practice of palynology. Optical superresolution methods would allow researchers to more easily examine pollen specimens that are already mounted in palynological slides (and therefore not readily accessible for EM), as well as analyze rare reference and fossil material that would otherwise be destroyed by EM preparation protocols such as sputter coating and microtome sectioning. The use of optical superresolution would further allow the seamless visualization of a pollen grain at multiple resolutions, from standard transmitted light to superresolution, permitting the morphology observed under different methods to be easily interpreted. This highly efficient and timesaving workflow would enable more detailed analyses of pollen morphology and investigations of the biological affinity of unknown fossil types. Theoretically, all significant pollen types within a pollen sample could be identified with the assistance of superresolution microscopy.

In this article, we demonstrate the potential of two emerging superresolution optical microscopy techniques—Superresolution Structured Illumination Microscopy (SR-SIM) (Gustafsson et al., 2008) and Airyscan Confocal Superresolution Microscopy (Airyscan or Image Scanning Microscopy; Muller & Enderlein, 2010; Sheppard, Mehta, & Heintzmann, 2013; Weisshart, 2014)—to capture morphological detail below the diffraction limit from both modern reference and fossil pollen specimens. We highlight the effectiveness of each technique using a range of pollen morphotypes and compare new contrast-enhancing fluorescent staining techniques and embedding media.

2 | MATERIALS AND METHODS

2.1 | Procurement and preparation of pollen specimens

We used both fossil and modern reference material in our study. For our modern material, we used three extant species with distinct and varied ornamentation and structure of the exine (pollen wall): *Croton hirtus* (Euphorbiaceae), *Dactylis glomerata* (Poaceae), and *Helianthus* sp. (Asteraceae). The morphological features of these species ranged in size from tens of microns to tens of nanometers. *C. hirtus* had been previously examined using detailed optical microscopy by Sivaguru et al. (2012) and *D. glomerata* surface texture was described using SEM by Mander et al. (2013). The morphology of *C. hirtus* is distinctive to *Croton*, with prominent elements approximately 500 nm in size (called clava) protruding from the surface and arranged in a *Croton* pattern (Punt et al., 2007). The thicker exine and more robust ornamentation of *Croton* pollen results in a high degree of light absorption (Sivaguru et al., 2012). *Dactylis glomerata* pollen, like that of other grasses, is characterized by a thin exine with minimal ornamentation visible under transmitted light. Under SEM, submicron areolae (polygonal islands) are visible in many species (Mander et al., 2013; Mander & Punyasena, 2014, 2016). Interspersed on the surface are nanoscale features of high relief, called granula (Mander et al., 2013; Mander & Punyasena, 2014, 2016). The most prominent features on *Helianthus* are the echinae (spines), typical of the Asteraceae family.

Pure *D. glomerata* pollen was procured from Sigma-Aldrich (St. Louis, MO). *Helianthus* sp. pollen was obtained as a prepared slide from Carolina Biological Supply (Burlington, NC), who stained the pollen using Phloxine B and mounted it in Practomount. *Croton hirtus* pollen was collected from herbarium specimens at the Smithsonian Tropical Research Institute, Panama and prepared following standard procedures outlined in Fægri et al. (1992). Pollen samples were incubated in potassium hydroxide to remove humic acids, hydrochloric acid to remove carbonates, and acetolysis to remove cellulose. *D. glomerata* samples were prepared using a modified procedure that excluded carbon-containing compounds (Nelson, Hu, & Michener, 2006). Our primary modification to standard palynological processing was the replacement of acetolysis with a 2-hr incubation in sulfuric acid.

The fossil material used in our study is from three sources. Holocene fossil pollen was obtained from a 500-year-old lake sediment sample from Lake Rutundu, located on the northeastern flank of Mt Kenya in eastern Africa (Urban et al., 2013), and the first set of Miocene fossil pollen is from a core in the Rubielos de Mora basin of northeastern Spain and dates to approximately 18–16 million years before present (Urban, Nelson, Jimenez-Moreno, and Hu, 2016). Both fossil samples were prepared following the same modified preparation procedure as *D. glomerata*. The final fossil sample is of Miocene material from northern Venezuela, and is approximately 16–12 million years old. Paleoflora Ltd., Colombia, prepared the samples. The specifics of the processing and embedding medium used are proprietary and unpublished, but roughly follow the standard preparation methods outlined in Fægri et al. (1992).

2.2 | Staining procedures for D. glomerata and fossil samples

The exine, or exterior encasing, of a pollen grain is naturally autofluorescent. However, the strength of the fluorescence and the resulting signal to noise ratio (SNR) varies with exine thickness. The microscopy methods analyzed in our study require samples with high SNR. Fluorescent labeling of pollen improves SNR, so our first set of experiments addressed the extent to which labeling could improve our images. We used *D. glomerata*, the pollen grain with the thinnest exine and lowest signal to noise ratio as our test sample, and the stain Periodic Acid-Schiff solution (PAS; Sigma-Aldrich, St. Louis, MO).

Based on these results detailed below, we chose to stain our *D. glomerata*, Lake Rutundu, and Rubielos de Mora samples with PAS before further analysis. (Our *Helianthus* material came labeled with Phloxine B and the thick exine of *C. hirtus* is highly fluorescent, so did not require a label.) All pollen was hydrated before the custom-made staining procedure. Pollen samples that were stained were washed a minimum of three times with ultrapure water and passed through 60 μm Pluriselect cell sieves (Pluriselect, San Diego, CA) inserted into a 50 mL Falcon tube to remove large debris, and then through 20 μm Pluriselect cell sieves to isolate the pollen. Pollen samples were incubated in periodic acid for a minimum of 8 hr followed by three washes in distilled water. The pollen was then incubated with Schiff's reagent for a minimum of 30 min or until the pollen turns from yellow-white to purple. Pollen was washed again to remove excess stain and to allow the color to fully develop. Staining was performed within the 20 μm Pluriselect cell sieves to minimize loss of material.

2.3 | Mounting procedures for D. glomerata and fossil samples

The stained pollen was either mounted in Hoyer's media (Anderson, 1954) or Eukitt (Electron Microscopy Sciences, Hatfield, PA). In our previous experiments with superresolution imaging, we discovered that the main criterion for successful preparation was using a solid medium with a refractive index close to that of glass (Wesseln, 2015). Hoyer's and Eukitt are two media that fulfill this criterion. Notably, silicone oil, perhaps the most popular embedding media for Quaternary palynological analysis, is not appropriate. The mobility of the grain, a desirable quality for manual manipulation and rotation in pollen analysis (Fægri et al., 1992), is not desirable for superresolution imaging. Minute vibrations affect the quality of the images. The large number of images needed to produce an SR-SIM image makes this technique particularly vulnerable to vibrations during imaging (Wesseln, 2015).

For Hoyer's, the pollen was dehydrated in the 20 μm Pluriselect cell sieves using a graded ethanol series of 70%, 80%, and 100%. The pollen was then transferred to a microcentrifuge tube where it was suspended in Hoyer's media. For Eukitt, the pollen was dehydrated in 20 μm Pluriselect cell sieves with a graded ethanol/xylene series of 70%, 80%, 100% ethanol followed by 2:1, 1:1, 1:2 solutions of ethanol: xylene. The pollen was then transferred to microcentrifuge tubes and incubated in 100% xylene with three drops of Eukitt to allow for infiltration of the mounting media overnight. For both mounting media, a 500 μL pipette was used to place a drop about 3–4 mm diameter on the slide. The sample drop was covered with a high-performance cover glass (0.17 mm thickness). Hoyer's mounted samples were dried at room temperature or placed on a hotplate set at 65°C for 1 week to promote drying. (Heat may sometimes promote bleeding of stains from samples into the medium.) Eukitt-mounted samples were dried at room temperature in a laboratory hood overnight.

2.4 | Measuring point spread functions of optical systems

Point spread functions (PSFs) were measured for each modality using 100 nm Tetraspeck fluorescent beads (Thermofisher, Catalog# T7279) prepared on a Zeiss high-performance cover glass with Prolong Gold antifade (Thermofisher, Eugene, OR) as the mounting medium. We have used 561 nm excitation laser for all modes with appropriate emission (570 LP) in each system using a Plan Apochromat 63× 1.4 NA (Carl Zeiss) objective. The LSM 880 was used for both confocal and Airyscan modes using the Airyscan detector (described below). The SR-SIM system was used to generate widefield and SR-SIM PSFs.

2.5 | Imaging pollen using confocal and airyscan superresolution microscopes

We used the LSM 880 with Airyscan (Carl Zeiss, Jena, Germany) system with GaAsP detectors (Gallium:Arsenide:Phosphide) for both confocal and Airyscan imaging. In the standard confocal approach, only one detector is used. The Airyscan represents a new laser scanning imaging technique much like confocal but with 32 detectors replacing the single photomultiplier detector of the standard confocal microscope and producing a two-fold signal to noise ratio (SNR) improvement over conventional detectors (Weisshart, 2014; Urban et al., this issue). The light path is illustrated in Figure 1A. In both Airyscan and conventional confocal modes, a 63× Plan Apochromat (1.4 NA) oil objective was used. In the confocal mode, the pinhole was set to 1.0 airy unit (AU). In the Airyscan superresolution mode, emission light was projected onto an array of 32 GaAsP detectors in a hexagonal pattern each representing 0.2 AU (Weisshart, 2014). These are arranged in three rings with a central detector. The complete array represented 1.25 AU from a sample. At a given time and laser position the signal from each detector goes to the appropriate pixel in the image. Reducing pinhole size from 1 to 0.2 AU improves the resolution by a factor of 1.4, using the point spread function (PSF) to dynamically reassign the photons gives a total improvement of 1.7 over the confocal resolution. The PSF refers to the image of each sub-diffraction and near diffraction fluorescent point source that defines the spatial resolution of the microscope (Allen, Ross, & Davidson, 2014; Habuchi, 2014; Jost & Heintzmann, 2013). The confocal and Airyscan image acquisition settings are provided in Table 1.

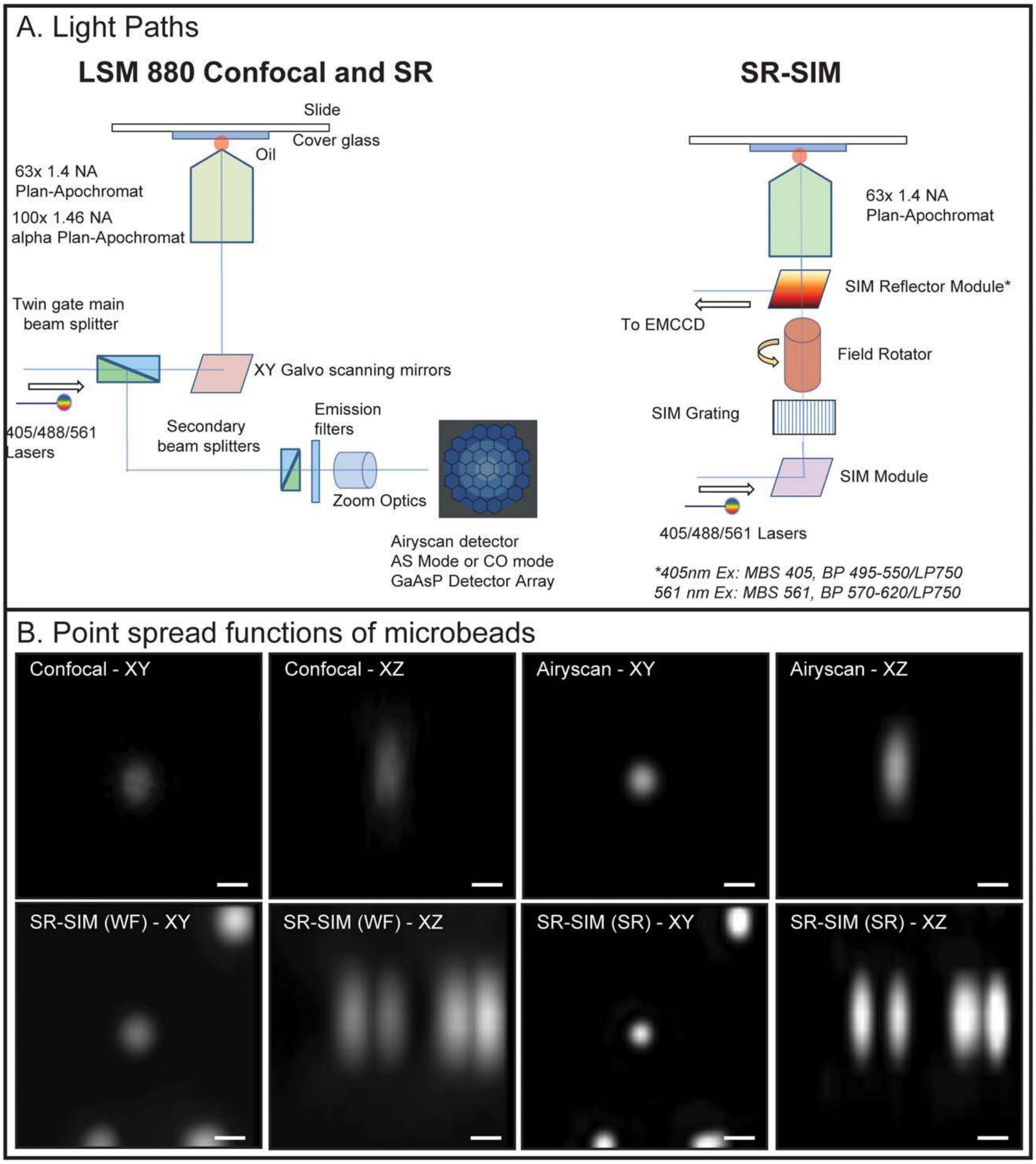

FIGURE 1 (A) Light paths for the LSM 880 [confocal and Airyscan Superresolution (SR)] and SR-SIM. AS, Airyscan; CO, Confocal; SIM, structured illumination microscopy. The Airyscan detector is a 32-channel GaAsP detector used in superresolution mode (AS) as well as confocal mode (CO). The SIM grating used for the study is 34 μm, but wavelength dependent grid frequencies are available from 28 to 54 μm and switched based on the excitation wavelength used. (B) Images of 100 nm Tetraspeck fluorescent beads used to measure point spread functions for each modality. Scale bars represent 0.2 μm. SR: Superresolution; WF, widefield. All images are collected from 561 nm excitation and 570–630 nm emission band pass. The full width at half maximum lateral resolution values for modalities are widefield: 259 nm; confocal: 204 nm; Airyscan: 161 nm and SR-SIM: 125 nm. Same bead set was shown between widefield-SR-SIM and confocal-Airyscan [Color figure can be viewed in the online issue, which is available at wileyonlinelibrary.com.]

TABLE 1 Summary of image acquisition techniques and methodology

Techniques	Confocal (GaAsP)	Airyscan	SR-SIM
Systems	LSM 880, Carl Zeiss, Jena, Germany	LSM 880, Carl Zeiss, Jena, Germany	ELYRA S1, Carl Zeiss, Jena, German
Objectives	63× Plan Apochromat DIC (1.4 NA) Oil, 100× 1.46 NA Alpha Plan Apochromat DIC with 1.4 NA Oil Condenser	63× Plan Apochromat DIC (1.4 NA) Oil, 100× 1.46 NA Alpha Plan Apochromat DIC with 1.4 NA Oil Condenser	63× Plan Apochromat DIC (1.4 NA) Oil, 100× 1.46 NA Alpha Plan Apochromat DIC with 1.4 NA Oil Condenser
Dimensions/(X,Y,Z in μm)	1,024 × 1,024 (0.04 × 0.04 × 0.1[a])	1,024 × 1,024 (0.04 × 0.04 × 0.1[a])	1,004 × 1,002 (0.037 × 0.037 × 0.1[a])
Emission wavelengths	Ex405; Em 420-480 + LP 605; Ex488; Em495-550 + LP 570	Ex405; Em 420-480 + LP 605; Ex488; Em495-550 + LP 570	Ex561; Em 570-620 + LP 750
Excitation wavelengths	405 nm, 488 nm, 561 nm	405 nm, 488 nm, 561 nm	406 nm, 488 nm, 561 nm
Detectors	Airyscan detector (Confocal Mode)	Airyscan detector (Airyscan Mode)	Andor Ixon 885 EMCCD
Digital Post-processing and Software	Subset of processed data planes, Max intensity projection, 3 × 3 median filter-Zen, Orthogonal projections–Autoquant X3	Airyscan module, Subset of processed data planes, Max intensity projection, 3 × 3 median filter -Zen, Orthogonal projections - Autoquant X3	Structured Illumination module, Subset of processed data planes, Max intensity projection, 3 × 3 median filter -Zen, Orthogonal projections - Autoquant X3

[a]Average length for z.

2.6 | Imaging pollen using Superresolution-structured illumination microscopy

The Elyra S1 SR-SIM light path (Carl Zeiss, Jena, Germany) is illustrated in Figure 1A. SR-SIM is a recently developed optical superresolution microscopy method with increasing applications in the life sciences (Habuchi, 2014; Han, Li, Fan, & Jiang, 2013; Huang, Bates, & Zhuang, 2010; Leung & Chou, 2011; Long, Robinson, & Zhong, 2014). It is a fluorescence technique with a light path similar to a widefield fluorescence microscope, but with a moving optical grid of parallel lines that is projected onto the sample in the lateral (XY) and axial (Z) directions. During standard SR-SIM image acquisition, five images of the sample are collected when the grid is repeatedly moved one fifth of the grid spacing along the X-axis. Moiré fringes are created by this grid pattern and the sample. The Moiré fringes are then transmitted through the objective to the camera. Moving the resulting image to Fourier space allows the original sample structure to be reconstructed by removing the known grid pattern from the Moiré fringes (Gustafsson et al., 2008). Image resolution on the Y-axis is improved by rotating the grid at predetermined angles to collect an isotropic improvement in resolution (Gustafsson, 2000; Gustafsson et al., 2008; Lukosz & Marchand, 1963; Sun & Leith, 1992). Because the grid projection is structured on the Z-axis, the optical sectioning resolution is improved two-fold compared with the standard confocal. Therefore, resolutions of 120 nm laterally (XY) and 250 nm axially (Z) can be achieved depending on the wavelength used (Allen et al., 2014; Dan, Yao, & Lei, 2014; Gustafsson, 2000; Gustafsson et al., 2008; Jost & Heintzmann, 2013; Kasuboski, Sigal, Joens, Lillemeier, & Fitzpatrick, 2012; Long et al., 2014).

In our study, we used the 34-μm gratings of the Zeiss Elyra S1 SR-SIM system to create near diffraction-limited lines for 561 nm light, by combining the +1, −1, and 0 diffraction orders in the back aperture of the objective. A theoretical lateral resolution of 140 nm is possible with this setting. This pattern was rotated to five pre-aligned angles and at each rotation the grating was moved five times to collect images with the grid in five phases, or positions. Thus, constructing a single plane of an SR-SIM image with five rotations and five phases per rotation required 25 images. For a typical pollen image Z-stack 4 μm in depth and with multiple axial sections taken at 130 nm steps, approximately 750 images were required for acquisition for a single wavelength of light [(3,900 nm/130 nm) × 25 images].

The Elyra S1 was calibrated for a 63× Plan Apochromat (1.4 NA) oil objective using PSF measurements from both sub-diffraction (50 nm) and near diffraction (170 nm) limited point source fluorescent beads supplied by the system manufacturer. The empirical PSFs were measured using these beads and the same wavelengths and objective used in this study. The Electron Multiplying Charge Coupled Device (EMCCD; Andor iXon 885) gain and exposure times were kept constant across specimens, but the laser power was set to optimize the quality of the image. The default SR-SIM image acquisition settings used are provided in Table 1.

2.7 | Image processing and analysis

Pollen samples were imaged with the three microscopy methods (standard confocal, Airyscan, and SR-SIM) as a series of axial images, or Z-stacks. The raw (confocal) and processed (SR-SIM and Airyscan) images were stored in the proprietary Zeiss CZI file format. Images of pollen grains were optimized for visualization by manually adjusting the minimum and maximum intensity values of the histogram in Zen, a program native to Zeiss microscopes. Subsets of focal planes were made to highlight various structures on the surface of the pollen grains. Line intensity profiles were obtained for the surface structures either linearly across an image or from location to location to highlight the resolution, signal and noise values of each modality. Some images were cropped to highlight specific areas of a given pollen grain to compare the retrieval of information from various modalities and before and after staining. Orthogonal maximum and single plane images of XY and XZ were produced using Autoquant X3 (Media Cybernatics, Bethesda,

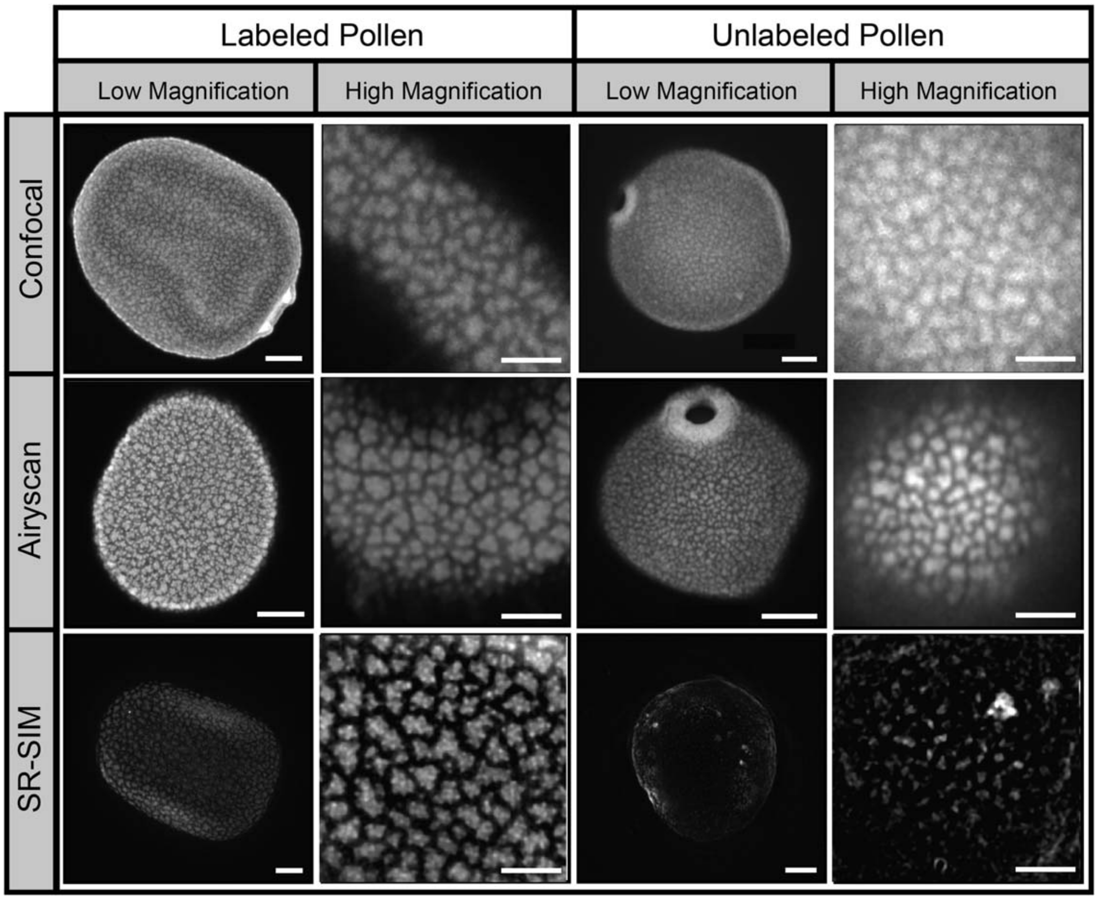

FIGURE 2 Low and high magnification comparisons of labeled (periodic acid-Schiff) and unlabeled *Dactylis glomerata* grains under the three modalities (Confocal, Airyscan, SR-SIM). For low magnification images, scale bars represent 5 μm. Scale bars for the corresponding high magnification images represent 2 μm. All low magnification images represent maximum intensity projections of all planes within the Z-stack. All high magnification images represent a subset of 3 axial planes.

MD). Videos of optical sections were made with the program Imaris Suite and Zen and stored in AVI format. Three-dimensional rendering algorithms of maximum intensity projections, blend projections, mixed projections of transparency and surface algorithms, and iso-surface projections were made after setting specific thresholds. FFT images were made in the program Image J (NIH Open Source software 2015) and pseudo-colored to highlight low and high frequency gain. For the FFT analysis, the average intensities of frequency values within an image (at an angle of 0° to the image center) were recovered using a 6-pixel wide line profile across the image center. At each horizontal pixel the intensity of the 6 pixels was averaged to give an intensity value to plot.

3 | RESULTS

3.1 | Preparation methods

In our preliminary experiments to determine the effects of processing and preparation, we first tested the effect of using PAS on our ability to image the fine structure of *Dactylis glomerata*. All of the imaging methods showed an increase in image quality with labeling (Figure 2; Supporting Information Movies S1 and S2). The areolae were sharper in the labeled sample for confocal, the lowest resolution method. In Airyscan, the granula were evident only in the labeled sample. Labeling most dramatically improved the results for SR-SIM. This is not surprising given the large number of images and high signal needed for SR-SIM imaging. Labeling improved the signal as indicated by the higher signal to noise ratio (Supporting Information Table S1) and reduced photobleaching. Both the areolae and granula were clearly visible in the labeled SR-SIM sample, with images closely resembling those from SEM (Mander et al., 2013). The unlabeled SR-SIM sample showed the well-defined edges of what could be the areolae, but the structural shape notably does not match SEM, Airyscan or the labeled SR-SIM images (Figure 2). We found minimal differences among the embedding media. We were able to successfully image material using Hoyer's, Eukitt, Practomount (for the commercially prepared *Helianthus* sp. samples), and an unknown solid medium (for the commercially prepared Miocene Venezuelan material).

Based on these results, we chose to stain our *D. glomerata* and two of our fossil samples with PAS before further analysis. The *Helianthus sp.* samples were commercially prepared and arrived stained with Phloxine B. Because of ease of preparation (Urban, Barclay, Sivaguru, &

Punyasena, 2016), samples that were prepared in-house were mounted in Eukitt.

3.2 | Performance comparison of optical systems using point spread functions

The full width at half maximum measurements performed using the 100 nm fluorescent beads showed a lateral resolution of 259 nm in widefield, 204 nm in confocal, 161 nm in Airyscan, and 125 nm for SR-SIM and are presented in Figure 1B. These results indicate that in practice, the SR-SIM provides a two-fold improvement in lateral resolution, while Airyscan results in an approximately 1.6 times enhancement in lateral resolution over diffraction-limited widefield fluorescence.

3.3 | Comparison of imaging methods

Maximum intensity and single plane images of the three pollen types (*Croton hirtus* [unlabeled], *Dactylis glomerata* [PAS], and *Helianthus* sp. [Phloxine B]), comparing the three imaging methods (confocal, Airyscan, and SR-SIM), are presented for both the XY and XZ orientations in Figure 3. The results demonstrate the differences in the resolution of pollen grains and imaging depth of each technique. We include a single XZ plane to show the morphological detail visible at increasing imaging depth. Intensity line profiles, measured across the XY projections, quantify the relative contrast. Because the cytoplasm remained intact in the *Helianthus* samples, which strongly absorbed the Phloxine B stain, the interior of the pollen grain was highly fluorescent. For this reason, our XY reconstruction of the Airyscan results includes a rendered three-dimensional shaded projection instead of a maximum intensity projection alone. The depth of penetration was most affected by the degree of absorption by the pollen exine, which varied by taxon. However, Airyscan appears to have the greatest depth of penetration.

Figure 4 compares the ability of each microscopy method to capture high-resolution details of the pollen surface. Line profiles in this figure are constructed by measuring pixel intensities in an irregular path that zigzagged from the center of one morphological feature to the next. This was done in order to emphasize the contrast of features from background within an image. For the high-magnification images of *D. glomerata*, two separate sets of layers were chosen to emphasize the patterning of the areolae and granula. The fine-scale optical sectioning possible with the SR-SIM further reveals that the patterning of the granula is tied to the collumellate structure of the pollen wall. Both Airyscan and SR-SIM show improvements in the morphological detail recovered, but SR-SIM shows morphological detail not evident with the confocal or Airyscan. Whether this morphological detail is real or artifact is discussed later in the article.

Figure 5 illustrates the impressive optical sectioning capabilities of both superresolution methods. The profile and structure of the echinae of *Helianthus* sp. and clava of *C. hirtus* are clearly visible with Airyscan (Figure 5A, B). These are relatively large structures, for example, clava are approximately 16.8 μm in size on average. The additional resolution of the SR-SIM is needed to distinguish the fine-scale structures (tectal columellae, ~250 nm) that compose the pollen wall of *D. glomerata* (Figure 5D).

The increase in resolution delivered by the SR-SIM and Airyscan compared with the confocal is quantified in in Figure 6. Low magnification and high magnification images of *D. glomerata* are presented along with fast Fourier transforms (FFTs) of the high-resolution images. Circles representing 250 nm resolution, the standard limit of optical resolution, have been added to the FFTs of each image to aid in comparison (Figure 6A). Standard confocal is diffraction-limited. Airyscan approaches this level of resolution. SR-SIM surpasses it. To more directly compare the resolution capabilities of each microscopy technique, we overlay cross-sections taken through the center of the FFT intensity plots (Figure 6B). Intensity values were averaged across six pixels perpendicular to the y-axis cross-section. The results demonstrate that the Airyscan and the SR-SIM outperformed the standard confocal across the entire spectrum of feature sizes present in the *D. glomerata* image. Although the Airyscan appears to have the greater ability to distinguish larger features (1–3 cycles/μm, or 1,000–333 nm in size), the SR-SIM is better able to detect smaller features (6–8 cycles/μm, or 166–125 nm in size).

4 | DISCUSSION

4.1 | Taxon-dependent results

The most effective technique for visualizing pollen features depended on feature size. For *C. hirtus*, the shape and arrangement of the clava were visible under all three imaging methods, but our best images for this type of pollen grain came from the Airyscan. The images showed improved resolution as demonstrated by the sharpness of features in the maximum intensity projection, the wider, more distinct, valleys in the intensity plot, and clarity of the clava profiles in the single XZ plane (Figure 3; Supporting Information Movie S5). Airyscan also clearly imaged the muri, the interconnecting ridges supporting the clava, which were not visible with the SR-SIM but were suggested, although not definitive, in the confocal (Figure 5B; Supporting Information Movie S5). Although the SR-SIM penetrated deeper into the grain than the other methods (Figure 3), the edges of the clava were overemphasized and showed strong variations in fluorescence intensity (Figure 4; Supporting Information Figure S1). These intensity variations were also suggested in the Airyscan images (Figure 4; Supporting Information Movie S5) and became more apparent with extremely long Airyscan imaging times. This suggests that the variations in intensity may be real and reflect differences in the autofluorescence properties within the clava that may reflect true structure.

In contrast, the thinner exine, smaller size of surface features, and lower optical absorption of *D. glomerata* made the SR-SIM more effective. At low magnification, the areolae were visible under all three methods, but were the most distinct deeper in the Z-stack with the SR-SIM (Figure 3). Airyscan, however, retains more of the information originating from the sample than the SR-SIM, resulting in better contrast with increasing depth (Figures 3 and 5; Supporting Information Movies S1 and S2). In comparison, the granula and underlying columellae cannot be sufficiently resolved in the confocal system, even after the critical application of fluorescent labeling (Figure 2). The contrast between the granula and areolae was only visible with twice the optical

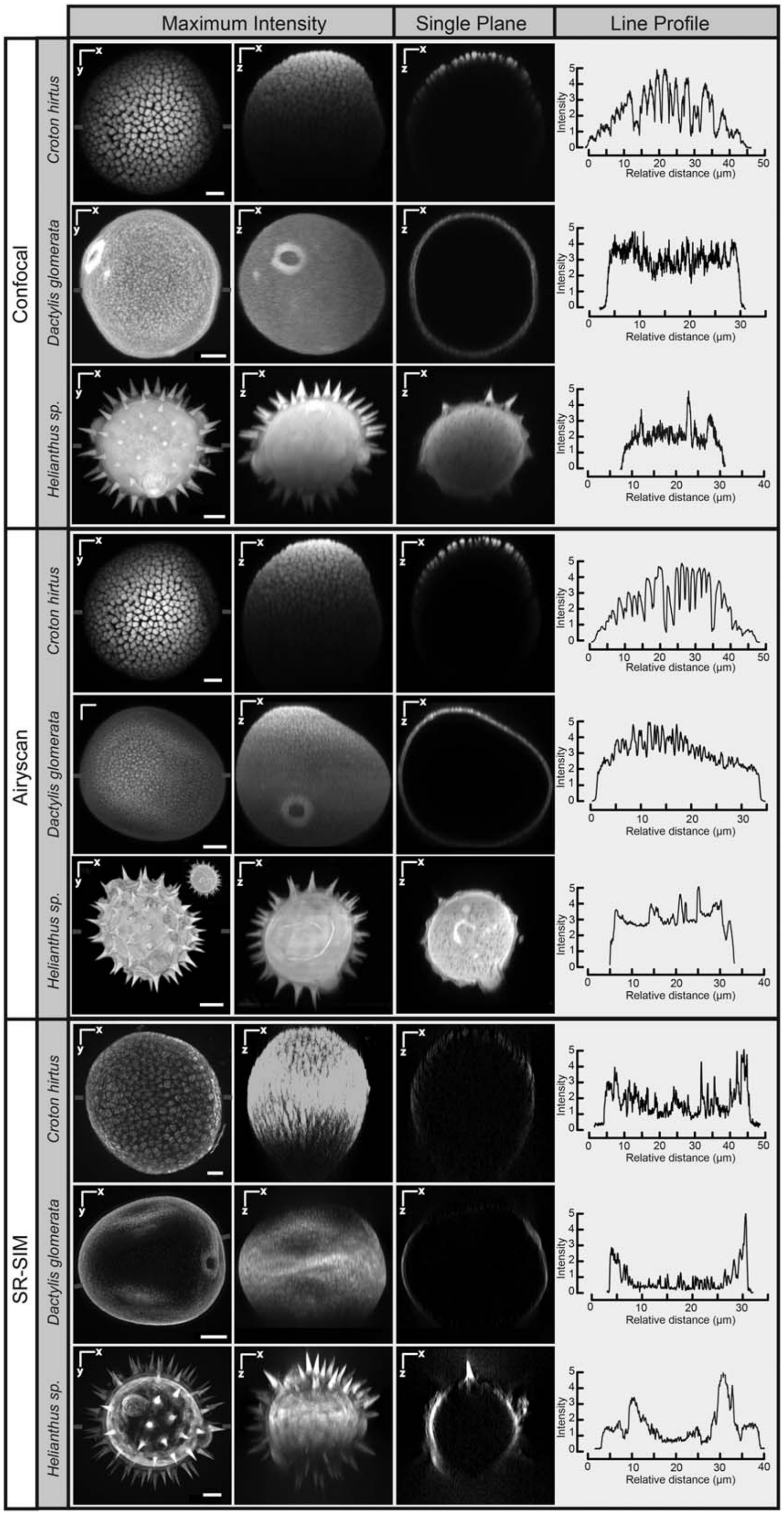

FIGURE 3 Low magnification images of each pollen type under the three modalities (confocal, Airyscan, SR-SIM). All images were cropped to fit the individual panels. Original image sizes are found in Table 1. Scale bars at the bottom right corner of each XY maximum intensity projection (MIP) image represent 5 μm. All images of a species for a given modality (i.e., each row) are shown at the same scale. The *Helianthus* XY projection for Airyscan is a 3D render (hybrid, see methods for details) of the grain, with the inset being the true MIP. The interior space of the grain has higher intensity than the surface masking the surface features. The line profiles represent intensity values measured across the middle of the pollen grain, marked by the two short gray lines on the middle left and middle right of the corresponding XY projections. To simplify line profile figures, all intensities were normalized to a scale between 0 and 5.

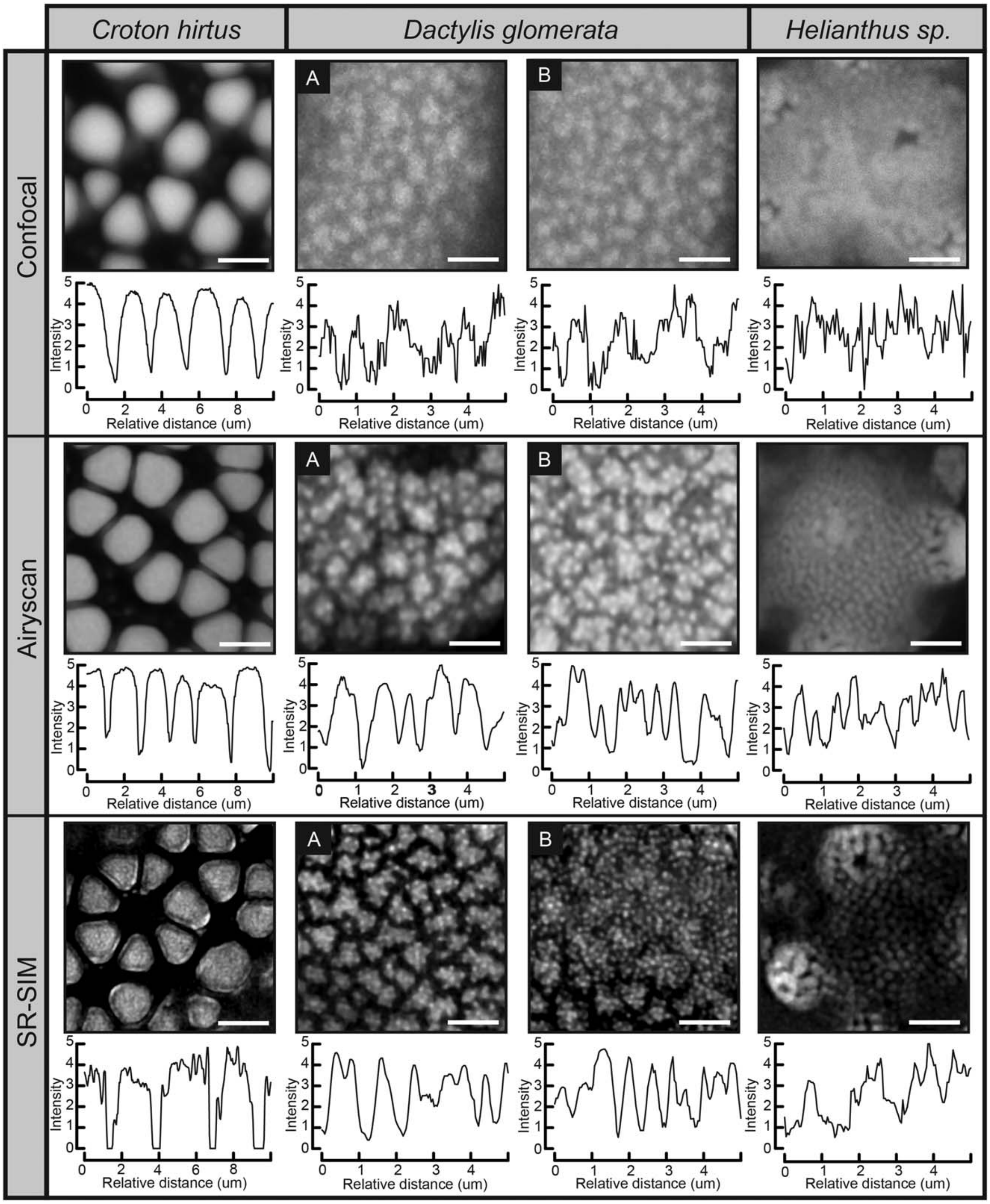

FIGURE 4 High magnification images of each pollen type under the three modalities (confocal, Airyscan, and SR-SIM). All images represent the maximum intensity projection (MIP) of a subset of 3 axial planes. Scale bars represent 2 μm. For *Dactylis glomerata*, the major structures are best represented using two different sets of MIPs of three planes. (A) Represents the three surface planes of the grain. (B) Represents the three planes below (A). The line profiles were generated using each MIP image by drawing lines between the major structures. To simplify line profile figures, all intensities were normalized to a scale between 0 and 5.

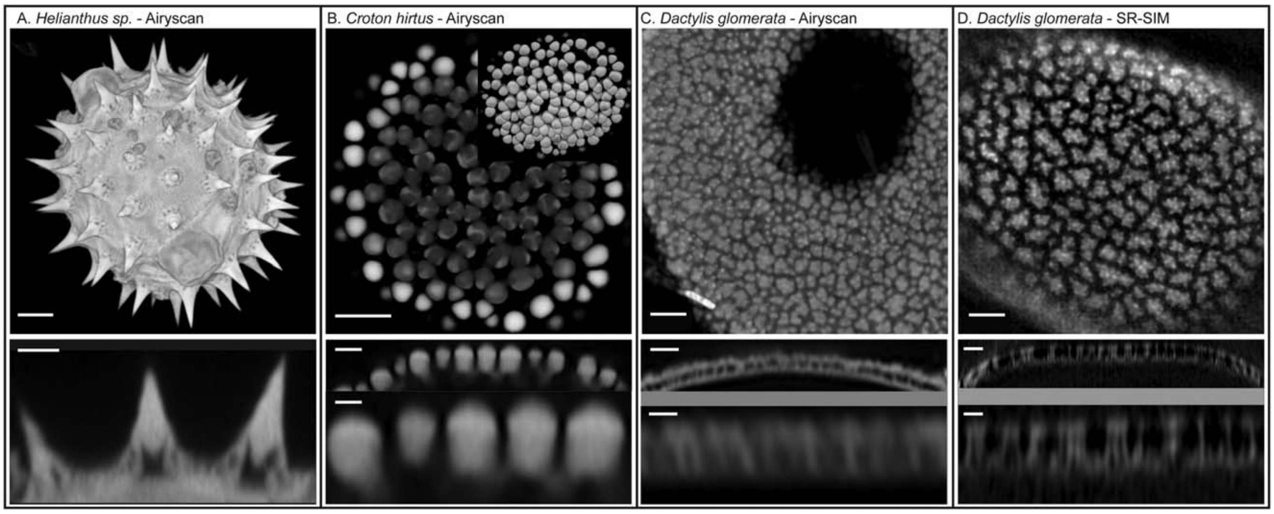

FIGURE 5 The internal structures *Helianthus* sp., *Croton hirtus*, and *Dactylis glomerata* under Airyscan and SR-SIM modalities. (A, top): Hybrid 3D projection of *Helianthus* sp. Scale bar represents 5 μm. (A, bottom): XZ cross section through the exine. Scale bar represents 2 μm. (B, top): surface of a *Croton hirtus* grain showing how the muri connect the individual clava. Scale bar represents 5 μm. Inset shows the maximum intensity projection (MIP) of the outside of the same grain. (B, bottom): XZ cross-section through the grain showing individual clava. Scale bar represents 2 μm for the upper cross-section and 0.5 μm for the lower. (C, top): A 10-plane MIP subset of a *Dactylis glomerata* grain using Airyscan. Scale bar represents 5 μm. (C, bottom): XZ cross-section through the grain showing details of the tectum, columellae, and foot layer. Scale bar represents 2 μm for the upper cross-section and 0.5 μm for the lower. (D, top): A 10-plane MIP subset of a *Dactylis glomerata* grain using SR-SIM. Scale bar represents 5 μm. (D, bottom): XZ cross section through the grain showing details of the tectum, columellae and foot layer. Scale bar represents 2 μm for the upper cross-section and 0.5 μm for the lower.

resolution (the SR-SIM) or when all the photons are collected, reassigned, and deconvolved (the Airyscan) (Figure 4). The columellate structure of the pollen wall, however, was most distinct with the SR-SIM. The differences between the two superresolution techniques were further emphasized by the FFT analysis and frequency spectrum of the same labeled *D. glomerata* pollen grain (Figure 6). Under identical brightness and spatial frequency intensity and distribution, the amplitude of spatial frequencies for the Airyscan was similar to the SR-SIM at the lower spatial frequencies (1–3 cycles/μm or 1,000–333 nm) that are expected by theory (Figure 6B). At higher spatial frequencies (4–8 cycles/μm or 250–125 nm), the SR-SIM was slightly better at capturing smaller features, such as the granula and columellae. Both Airyscan and SR-SIM systems revealed these details only after labeling the pollen with the fluorescent stain PAS (Sivaguru et al., 2015).

Due to differences in processing methods, the cytoplasm remained intact in the *Helianthus* samples. This internal matrix strongly absorbed the Phloxine B stain and was highly fluorescent. For this reason, our XY reconstruction and supplemental movie of the Airyscan results uses a rendered three-dimensional mixed projection (mixture of transparency and surface projections) projection instead of a maximum intensity projection alone (Figure 3; Supporting Information Movie S4). The signal introduced by the presence of cytoplasm would have been removed if the pollen had been processed using standard palynological processing techniques (Fægri et al., 1992). Despite this, significant morphological detail is still apparent in the *Helianthus* images. At high magnification, the Airyscan and SR-SIM appear to capture the scabrate surface texture of *Helianthus* sp. not visible with confocal (Figure 4; Supporting Information Movies S3 and S4). The confocal XZ images show echinae with blunted tips resulting from the difference in the XY and XZ resolution (Figure 3). This distortion is less apparent with the higher resolution Airyscan and SR-SIM, which better capture the true shape of the echinae in three dimensions (Supporting Information Movies S3 and S4). At high magnification, the single plane Airyscan XZ projection captures a detailed cross-section of the exine, with the tectum, columellae, and foot layer clearly differentiated (Figure 5A; Supporting Information Movies S3 and S4). The SR-SIM, however, had difficulty imaging these structures due to optical distortions of the grid resulting from the irregular pollen morphology. When the index of refraction of the pollen sample varies from the index of refraction of the mounting medium, the pollen structures act as lenses and distort the optical grid. The result is a distorted image of the pollen structures.

Taken together, the results suggest that SR-SIM excels at capturing small features (250–120 nm) on samples with a high signal to noise ratio, without irregular features that distort the grid pattern (Figure 3). In contrast, the Airyscan is better able to resolve images of unlabeled pollen, with a lower signal to noise ratio. These features need to be larger (>150 nm) (e.g., *C. hirtus*) because of the lower resolution of Airyscan. It was nearly impossible to effectively resolve the morphology of unlabeled *D. glomerata* grains with the SR-SIM given the large number of images and high signal to noise ratio needed for the technique. However, areolae (but not granula) were still clearly visible with the Airyscan. Thus, the Airyscan appears to be the better choice when only unlabeled samples are available (e.g., archived slides and samples). And while the Airyscan does not have the resolution of the SR-SIM, it can act as an independent check of the SR-SIM to ensure that the features in SR-SIM are not an artifact of distortion (Supporting Information Figure S1).

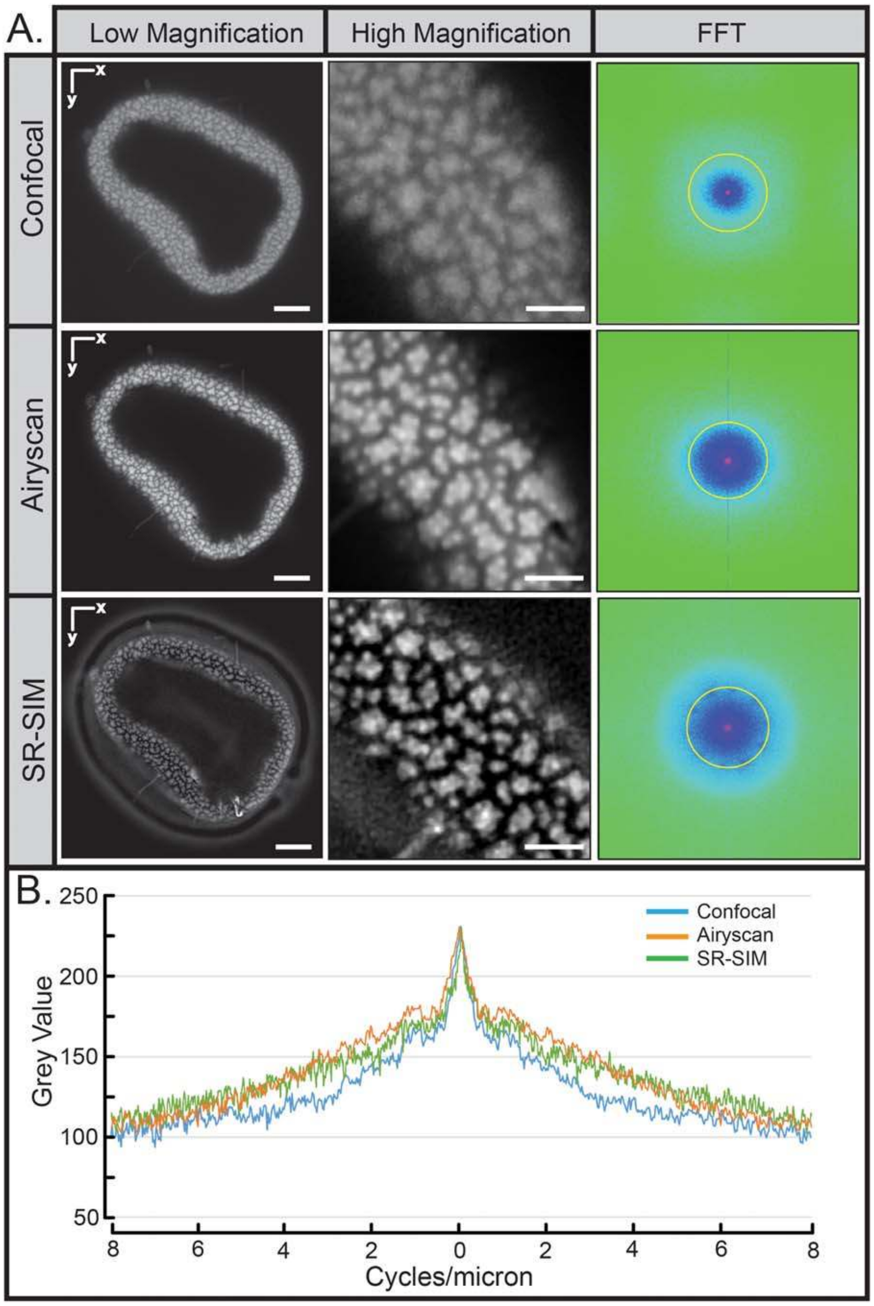

FIGURE 6 (A) Low and high magnification maximum intensity projection images of a three-plane subset of the same grain of *Dactylis glomerata* and the pseudocolored Fast Fourier Transform images across the three modalities (confocal, Airyscan, SR-SIM) of the high-magnification image. Color represents intensities from high (red) to low (green). Fast Fourier Transform (FFT) data were generated using the low magnification whole pollen images and the yellow circle represent spatial frequency of 4 cycles/micron or 250 nm. For low magnification images, scale bars represent 5 μm. The same scale bar represents 2 μm for the corresponding high magnification image. (B) Frequency spectra generated from the FFT images, comparing the transfer functions of each technique. The spectra are averages of 6-pixel wide lines drawn across the FFT image centers. The X-axis is the transferred frequencies in cycles per micron (e.g., 8 cycles represent 125 nm) and the Y-axis is the averaged intensity in 8-bit grayscale [Color figure can be viewed in the online issue, which is available at wileyonlinelibrary.com.]

4.2 | The potential of optical superresolution

Our images demonstrate the tremendous potential of optical superresolution methods for pollen analysis. The surface images from both the Airyscan and SR-SIM rival SEM for features larger than 120 nm. Additionally, the XZ sectioning capability of these optical techniques allows the internal structure of the pollen wall to be visualized. Internal and external structures can be viewed and correlated within the same specimen (the example of *C. hirtus* shown in Figure 5B; Supporting Information Movies S5 and S6). This integrated morphological analysis is not possible with current EM approaches to pollen analysis.

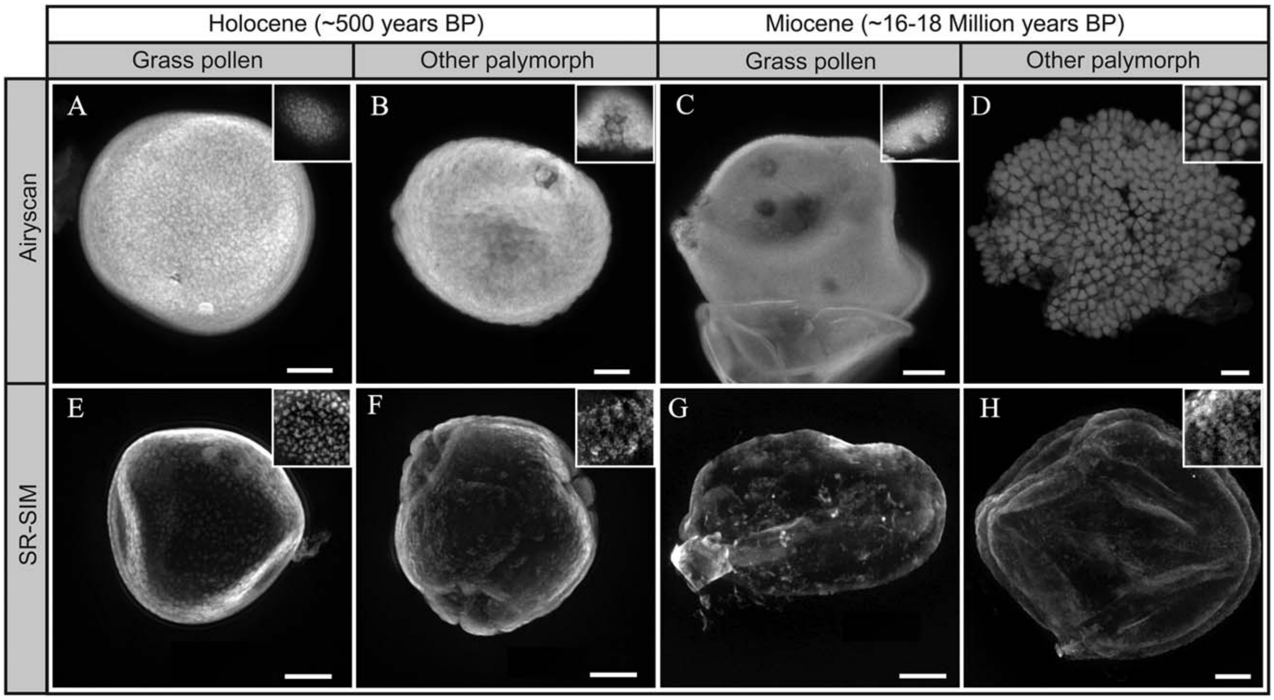

FIGURE 7 Representations of subfossil (Holocene) and fossil pollen (Miocene) imaged with Airyscan and SRSIM modalities. Scale bars represent 5 μm. Insets show 7.4 μm-wide cropped maximum intensity projection (MIP) images (subset of 3 axial planes) that emphasize surface texture. With the exception of (D) all grains were mounted in Hoyer's and labeled with periodic acid-Schiff (PAS). Mounting medium for (D) is unknown and it is unlabeled. (A, E) Poaceae (grass) grain from Lake Rutundu, Kenya. (B) *Celtis* sp. grain from Lake Rutundu, Kenya. (C) Poaceae grain from Rubielos de Mora Basin, Spain. (D) Croton-type grain from Urumaco Formation of Venezuela. (F) *Hagenia abyssinica* grain from Lake Rutundu, Kenya. (G) Poaceae (grass) grain from Rubielos de Mora basin, Spain. (H) Euphorbiaceae-type grain from Rubielos de Mora basin, Spain.

The ability of Airyscan and SR-SIM to work with standard microscope slides also provides a mechanism for a higher throughput approach to the taxonomic analyses of pollen samples, as critical morphological detail can be rapidly imaged and interpreted. This would potentially allow for more specific taxonomic classifications as a matter of routine for problematic groups, like the grasses, where critical morphological differences are smaller than the diffraction limit of 200–250 nm (Mander et al., 2013; Mander & Punyasena, 2014, 2016). Our results for *D. glomerata* demonstrate that surface features such as the patterning of the granula and shape of the areolae are visible with both the Airyscan and SR-SIM, and the three-dimensional shape and height of the granula are visible in cross-section.

Finally, Airyscan and SR-SIM are two superresolution methods that can be directly applied to naturally autofluorescent fossil samples. Figure 7 demonstrates the quality of images that can be achieved with subfossil (∼500 years old) and fossil (16–18 million years old) material (Figure 7). Two examples of fossil specimens (Figure 7C,D) were prepared by a commercial processing facility using a variation of the standard palynological processing methods developed for transmitted brightfield microscopy. The images that resulted are comparable to our modern reference material that was not labeled explicitly for fluorescence imaging. We prepared the remaining material expressly for superresolution imaging, including labeling these specimens with PAS (Figure 7A,B,E–H). The use of fluorescent stains augmented the signal. This is especially evident for the Holocene (∼500 years before present) grass pollen (Figure 7A,E insets) which show distinct surface ornamentation that is on par with that of a modern specimen. However, in the less robust Rubielos de Mora grass pollen, smaller scale morphological features appear less distinct, despite the use of fluorescent stain (Figure 7G). These specimens were likely strongly altered by diagenetic processes during fossilization. In this case, superresolution captures the taphonomic history of this specimen, rather than its taxonomic identity.

Overall, our images support the argument that Airyscan and SR-SIM are both viable techniques for the study of pollen morphology—whether it is in the context of paleoecology, pollen development, or plant systematics. The results provided by the two superresolution techniques, however, are not identical, but complementary. SR-SIM performs best only when a sample is thin and has a relatively high signal to noise ratio. The Airyscan performs better than SR-SIM for samples that have a lower signal to noise ratio or have structures that distort the optical grid (e.g., the echinae of *Helianthus*). Airyscan, however, never achieves the resolution of SR-SIM under optimal conditions (161 nm for the former vs. 125 nm for the latter). The appropriateness of a given technique ultimately depends on the nature of the morphological characters of interest, the light absorption characteristics of the pollen grain itself, image acquisition and processing parameters, and finally, the effectiveness of sample preparation methods. The use of a solid medium is critical, particularly for the SR-SIM. Labeling is vital for thin walled specimens with low signal to noise, as in the case of *D. glomerata*.

The nature of Airyscan and SR-SIM is very different from EM. SEM captures information from only the very surface of a specimen, whereas Airyscan and SR-SIM, as optical microscopy methods, are potentially able to reveal intricate, internal structures. Due to the nature of optical sectioning, this internal information is three-dimensional (Figure 5). As a result, some of the texture that is visible in the optical superresolution images, which may not be not visible in corresponding SEM images, potentially represent morphological features that are located within the pollen wall, rather than on its surface. For some samples, SR-SIM appears more prone to artifactual imaging (e.g., rings on *C. hirtus* clava or distorted areolae in unlabeled *D. glomerata*; Supporting Information Figure S1). Airyscan, therefore, should be used to corroborate SR-SIM data. The 161 nm resolution of the Airyscan is coarser than the 125 nm resolution of the SR-SIM, but the images will be more comparable than those from a standard confocal (Figure 1B). Further research interpreting superresolution optical microscopy images is needed to determine the nature of features that are only visible using SR-SIM and Airyscan. Establishing feature-to-feature correlations between superresolution images and scanning electron micrographs of biological structures is difficult, but detailed morphological analyses over a larger morphological range of pollen specimens using SEM, TEM, SR-SIM, and Airyscan would establish the degree to which these different methods capture the same or alternative morphological details.

An additional future challenge is to integrate superresolution techniques such as SR-SIM with semi- and fully-automated pollen and spore classification systems such as the Classifynder (Holt et al., 2011) and ARLO (Punyasena et al., 2012; Tcheng, Nayak, Fowlkes, & Punyasena, 2016), so that morphological data from below the diffraction limit of light can be collected and analyzed using high-throughput methodologies. The combination of superresolution microscopy with new approaches to computer vision and image analysis will allow even the smallest scale morphological differences among pollen and spores to be incorporated into the study of plant morphology and diversity.

ACKNOWLEDGMENTS

We thank Kelly Hardison (Carolina Biological Supply, Burlington, NC) for help with the custom-mounted labeled pollen of *Helianthus*; Austin Cyphersmith (University of Illinois, IGB core facilities) for help with data collection; and Carlos Jaramillo (Smithsonian Tropical Research Institute) and Alejandra Restrepo (University of Illinois) for allowing us access to the Urumaco, Venezuela material. We thank the editor and the reviewers for their comments, which substantially improved the manuscript. Support for MS, GF, MAU, CJW, and SWP provided by an NSF Advances in Bioinformatics grant (DBI-1262561) to SWP. Author contributions: MS, GF, and SWP designed the experiments. Data were collected by MS and MAU. Preliminary data collected by CJW and LM. Manuscript written by SWP, GF, and MAU, with contributions from MS, CJW, and LM.

REFERENCES

Allen, J. R., Ross, S. T., & Davidson, M. W. (2014). Structured illumination microscopy for superresolution. *ChemPhysChem Review*, *15*, 566–576.

Anderson, L. E. (1954). Hoyer's solution as a rapid permanent mounting medium for bryophytes. *The Bryologist*, *57*, 242–244.

Andersen, T. S., & Bertelsen, F. (1972). Scanning electron microscope studies of pollen of cereals and other grasses. *Grana*, *12*, 79–86.

Chaturvedi, M., Datta, K., & Nair, P. K. K. (1998). Pollen morphology of oryza (poaceae). *Grana*, *37*, 79–86.

Dan, D., Yao, B., & Lei, M. (2014). Structured illumination microscopy for superresolution and optical sectioning. *Chinese Science Bulletin*, *59*, 1291–1307.

Fægri, K., Iversen, J., & Kaland, P. E. (1992). *Textbook of pollen analysis* (4th ed.; 340 p). New York: The Blackburn Press.

Gustafsson, M. G. (2000). Surpassing the lateral resolution limit by a factor of two using structured illumination microscopy. *Journal of Microscopy*, *198*, 82–87.

Gustafsson, M. G., Shao, L., Carlton, P. M., Wang, C. J., Golubovskaya, I. N., Cande, W. Z., Agard, D. A., & Sedat, J. W. (2008). Three-dimensional resolution doubling in wide-field fluorescence microscopy by structured illumination. *Biophysical Journal*, *94*, 4957–4970.

Habuchi, S. (2014). Super-resolution molecular and functional imaging of nanoscale architectures in life and materials science. *Frontiers in Bioengineering and Biotechnology*, *2*, 1–13.

Han, R., Li, Z., Fan, Y., & Jiang, Y. (2013). Recent advances in super-resolution fluorescence imaging and its applications in biology. *Journal of Genetics and Genomics*, *40*, 583–595.

Heintzmann, R., & Ficz, G. (2006). Breaking the resolution limit in light microscopy. *Briefings in Functional Genomics and Proteomics*, *5*, 289–301.

Hesse, M., Halbritter, H., Weber, M., Buchner, R., Frosch-Radivo, A., Ulrich, S., & Zetter, R. (2009). *Pollen terminology: An illustrated handbook* (266 p). Vienna: Springer-Verlag.

Huang, B., Bates, M., & Zhuang, X. (2009). Super-resolution fluorescence microscopy. *Annual Review of Biochemistry*, *78*, 993–1016.

Holt, K., Allen, G., Hodgson, R., Marsland, S., & Fenley, J. (2011). Progress towards an automated trainable pollen location and classifier system for use in the palynology laboratory. *Review of Palaeobotany and Palynology*, *167*, 175–183.

Jost, A., & Heintzmann, R. (2013). Superresolution multidimensional imaging with structured illumination microscopy. *Annual Review Materials Research*, *43*, 261–282.

Kasuboski, J. M., Sigal, Y. J., Joens, M. S., Lillemeier, B. F., & Fitzpatrick, J. A. J. (2012). Super-resolution microscopy: A comparative treatment. *Current Protocols in Cytometry*, *2*, 1–24.

Leung, B. O., & Chou, K. C. (2011). Review of super-resolution fluorescence microscopy for biology. *Applied Spectroscopy*, *65*, 967–980.

Long, B. R., Robinson, D. C., & Zhong, H. (2014). Subdiffractive microscopy: Techniques, applications, and challenges. *Wiley Interdisciplinary Reviews: Systems Biology and Medicine*, *6*, 151–168.

Lukosz, W., & Marchand, M. (1963). Optischen abbildung unter überschreitung der beugungsbedingten auflösungsgrenze. *Journal of Modern Optics*, *10*, 241–255.

Mander, L., & Punyasena, S. W. (2014). On the taxonomic resolution of pollen and spore records of earth's vegetation. *International Journal of Plant Science*, *175*, 931–945.

Mander, L., & Punyasena, S. W. (2016). Grass pollen surface ornamentation: A review of morphotypes and taxonomic utility. *Journal of Micropalaeontology*, *35*, 121–124. First published online December 23, 2015, doi: 10.1144/jmpaleo2015-025

Mander, L., Li, M., Mio, W., Fowlkes, C. C., & Punyasena, S. W. (2013). Classification of grass pollen through the quantitative analysis of surface ornamentation and texture. *Proceedings of the Royal Society B*, *280*, 20131905.

Muller, C. B., & Enderlein, J. (2010). Image scanning microscopy. *Physical Review Letters*, *104*, 198–101.

Nelson, D. M., Hu, F. S., & Michener, R. H. (2006). Stable-carbon isotope composition of poaceae pollen: An assessment for reconstructing C_3 and C_4 grass abundance. *The Holocene*, *16*, 819–825.

Page, J. (1978). A scanning electron microscope survey of grass pollen. *Kew Bulletin*, *32*, 313–319.

Peltre, G., Cerceau-Larrival, M.-T., Hideux, M., Abadie, M., & David, B. (1987). Scanning and transmission electron microscopy related to immunochemical analysis of grass pollen. *Grana*, *26*, 158–170.

Punt, W., Hoen, P., Blackmore, S., Nilsson, S., & Le Thomas, A. (2007). Glossary of pollen and spore terminology. *Review of Palaeobotany and Palynology*, *143*, 1–81.

Punyasena, S. W., Tcheng, D. K., Wesseln, C., Pietra, P.G. (2012). Classifying black and white spruce pollen using layered machine learning. *New Phytologist*, *196*, 937–944.

Reimer, L. & Kohl, H. (2008). *Transmission electron microscopy: Physics of image formation* (590 p). New York: Springer-Verlag.

Sheppard, C. J. R., Mehta, S. B., & Heintzmann, R. (2013). Superresolution by image scanning microscopy using pixel reassignment. *Optics Letters*, *38*, 2889–2892.

Sivaguru, M., Mander, L., Fried, G., & Punyasena, S. W. (2012). Capturing the surface texture and shape of pollen: A comparison of microscopy techniques. *PLoS ONE*, *7*, e39129.

Sivaguru, M., Fried, G., Sivaguru, B. S., Sivaguru, V. A., Lu, X., Choi, K. H., . . . Sadayappan, S. (2015). Cardiac muscle organization revealed in 3-D by imaging whole-mount mouse hearts using two-photon fluorescence and confocal microscopy. *Biotechniques*, *59*, 295–308.

Sun, P., & Leith, EN. (1992). Superresolution by spatial-temporal encoding methods. *Applied Optics*, *31*, 4857–4862.

Tcheng, D. K., Nayak, A. K., Fowlkes, C. C., & Punyasena, S. W. (2016). A visual recognition software application for binary classification and its application to spruce pollen identification. *PLoS ONE*, *11*(2):e0148879.

Traverse, A. 2007. *Paleopalynology* (2nd ed.; 813 p). The Netherlands: Springer.

Urban, M. A., Nelson, D. M., Kelly, R., Ibrahim, T., Dietze, M., Pearson, A., & Hu, F. S. (2013). A hierarchical bayesian approach to the classification of C_3 and C_4 grass pollen based on SPIRAL $\delta^{13}C$ data. *Geochemica et Cosmochemica*, *121*, 168–176.

Urban, M. A., Barclay, R. S., Sivaguru, M., & Punyasena, S. W. (2016). Cuticle and subsurface ornamentation of intact plant leaf epidermis under confocal and super-resolution microscopy. *Microscopy Research and Technique*, (in press).

Urban, M. A., Nelson, D. M., Jiménez-Moreno, G., & Hu, F. S. (2016). Carbon isotope analyses reveal relatively high abundance of C4 grasses during early-middle miocene in southwestern Europe. *Palaeogeography*, *Palaeoclimatology*, *Palaeoecology*, *443*, 10–17.

Weiss, S. (2000). Shattering the diffraction limit of light: A revolution in fluorescence microscopy? *Proceedings of the National Academy of Sciences*, *97*, 8747–8749.

Weisshart, K. (2014). The basic principle of Airyscanning. Zeiss Technology Note, 22 p.

Wesseln, C. (2015). Imaging nanoscale pollen morphology with supperresolution structured illumination microscopy. MS Thesis, University of Illinois at Urbana-Champaign. 46 p.

SUPPORTING INFORMATION

Additional Supporting Information may be found in the online version of this article.

How to cite this article: Sivaguru M, Urban MA, Fried G, Wesseln CJ, Mander L, Punyasena SW. Comparative performance of airyscan and structured illumination superresolution microscopy in the study of the surface texture and 3D shape of pollen. Microsc Res Tech. 2018;81:101–114. https://doi.org/10.1002/jemt.22732